water

MDPI

Article

Trace and Rare Earth Element (REE) Geochemistry of Recently Formed Stromatolites at Lake Salda, SW Turkey

Mustafa Kaya [1], Belgin Aydin Yildirim [2], Mustafa Kumral [1] and Ahmet Sasmaz [2,*]

[1] Department of Geological Engineering, Istanbul Technical University, 34469 Istanbul, Turkey
[2] Department of Geological Engineering, Fırat University, 23119 Elazig, Turkey
* Correspondence: asasmaz@firat.edu.tr

Abstract: Stromatolites are the oldest recognized fossil recordings of life on Earth. Therefore, their study of them represents one of the most interesting topic that investigates the physio-chemical environmental conditions (formations and precipitations) at which the stromatolites formed. This work deals with the rare earth elements (REEs) geochemical characteristics and the redox-sensitive trace elements behavior of the stromatolites newly formed in Salda Lake, a closed system alkaline lake surrounded by serpentinite rocks in SW Turkey. The representative stromatolite samples collected from Salda Lake show higher contents of MgO (up to 41.5 wt.%), CO_2+OH (up to 56.6 wt.%), and MgO/CaO ratio (up to 42.2 wt.%) referring to the stromatolites had been controlled by microorganisms and deposited in subtidal areas having hydro-magnesite and aragonite mineralogy. The average trace element contents of the stromatolites are 8.4 ppm V, 0.09 ppm Cr, 3.50 ppm Co, 95.6 ppm Ni, 0.73 ppm Cu, 1.55 ppm Rb, 37.6 ppm Sr, 0.59 ppm Y, 17.7 ppm Zr, 3.60 ppm Nb, 21 ppm Ba, 0.05 ppm Hf, 3.5 ppm As, 0.02 ppm Cd, 0.05 ppm U, 0.05 ppm Th, 2.85 ppm Pb, and 6.60 ppm Zn. The Post-Archean Australian Shale (PAAS)-normalized REE patterns of the stromatolites reveal that the heavy REEs (HREEs) are enriched relative to the light REEs (LREEs) with highly negative Y and Ce-anomalies and positive Eu-anomalies. This refers to the stromatolites formed in predominantly oxidizing environmental conditions at partially warm lake waters. In addition, the hydromagnesite composition of the Salda Lake stromatolites indicates that they were precipitated from the waters influenced by Mg-rich meteoric waters fed from the serpentinite rocks around the Lake.

Keywords: rare earth element (REE) geochemistry; stromatolites; Lake Salda; SW Turkey

check for updates

Citation: Kaya, M.; Yildirim, B.A.; Kumral, M.; Sasmaz, A. Trace and Rare Earth Element (REE) Geochemistry of Recently Formed Stromatolites at Lake Salda, SW Turkey. *Water* **2023**, *15*, 733. https://doi.org/10.3390/w15040733

Academic Editor: Paolo Madonia

Received: 16 January 2023
Revised: 8 February 2023
Accepted: 9 February 2023
Published: 12 February 2023

1. Introduction

Salda Lake which located in the southwest of Turkey has attracted the attention of many scientists, this is because of its importance and similarity with the Jezero Crater Paleolake on Mars [1–6]. The stromatolite represents one of the oldest recognized fossils of a life recording on the Earth having laminated accretionary growth structures referring to the microbial origins [7–9]. Stromatolite morphogenesis is formed by the metabolic processes and microbial binding and trapping of sediments that promote mediate stromatolite lithification and mineral precipitation [10,11]. The metabolisms involved in the stromatolites contain sulfate reduction and anoxygenic or oxygenic photosynthesis [12]. However, some stromatolites have primarily formed by a biogenic precipitation [7,9]. In addition, the stromatolites have been commonly occurred in the lacustrine and seas with the weathered products of the different rock units [13–19]. Therefore, the geochemical properties and microfabrics of lacustrine stromatolites provide valuable information about paleoenvironmental changes in the continental environments [20].

Although extensive research studies have been performed on the stromatolites formed in different ages and environments, most of these studies focus on their genetic origin [7], their geomicrobiology [21], their limnology [22], their paleo-environmental environment [23], their petrographic and geochemical characterization [24], their precipitation

mechanisms [25] and their biomass content [26]. However, there is no more information about their physicochemical parameters and geochemical characteristics. Some of these works studied the trace element geochemistry of the depositional environment and formation conditions of stromatolites within an alkaline lake to define the redox conditions under which the stromatolites precipitated [27–35]. In the sedimentary environments, the behaviour of Ce and Eu gives valuable information about the redox conditions of depositional environments (i.e., shale normalized REE pattern). For example, the depletion of Ce indicates the oxygenation state of the H_2O, therefore the higher Ce concentrations are observed in anoxic environments referring to the Ce fractionation does not occur in these anoxic environments [28]. The trace element characteristics in marine carbonates and lacustrine deposits have been extensively studied [36–41]. Contrarily, geochemical properties and REE models of lacustrine carbonates have received limited interest [35,38,42–45] but no more studies on the geochemistry of the stromatolites. Here, we studied the precipitation conditions and formation of the stromatolites, the major oxide, and the trace and rare earth element contents of the stromatolites in the Lake Salda.

This study focuses on the major oxides, trace elements and REE patterns, Ce, Eu, Pr and Y anomalies and redox-sensitive trace elements to find out the physicochemical parameters and formation conditions of the precipitation environment of the stromatolites collected from Lake Salda, SW Turkey.

2. Geological Setting

Salda Lake was formed due to the tectonic activities forming a mid-size crater lake (Yeşilova district, Burdur, SW Turkey) (Figure 1). The lake area contains the autochthonous and allochthonous units (Figure 1) [46]. The allochthonous units consist of Marmaris Peridotite Nappe and Dunite Member, Kızılcadağ Ophiolitic Melange, Igdir Metamorphic Rocks, Dutdere Limestones and Orhaniye Formation. While the autochthonous units are represented by Çameli Formation, alluvium, and slope debris [47]. The Salda Lake is characterized by high alkalinity and higher pH content with the average of 9. The lake water gets contaminated as a result of the weathering of the serpentinized dunite and harzburgite rocks of the Upper Cretaceous Yesilova Ophiolites (Figure 1) which are widely distributed in the environment [13,21,22,48–50]. In addition, the proliferation of phytoplankton (diatom and blue and green algae) life which represents the most basic link of the food chain in a lake environment, causes the formation of biological reactions that will positively affect Mg-calcite precipitation. The hydro-magnesite [$Mg_5(CO_3)_4(OH)_2 \cdot 4H_2O$] in the Salda Lake was precipitated due to the retention of Mg element carried to the environment via meteoric waters by cyanobacteria and diatoms (i.e., blue-green algae). The Salda Lake Stromatolites range in size from a few centimeters to 70–80 cm in diameter forming circular, conchoidal or ellipsoidal shapes in water (Figure 2). In the outer part of the lake, the serpentinite rocks were manifested with the hydro-magnesite at their fracture systems (Figure 2). According to Balci, et al. [21], the meteoric and ground waters wash Mg from the ophiolitic rocks and ultramafic alluvial fans, as well as waters rich in Mg-HCO_3 with higher pH values. They then are transported to the lake in which the biological activities and cyanobacteria remove Mg^{+2} ions in the water out of the cell. These emphasized that hydro-magnesite precipitation was carried out by pulling on the cell membrane.

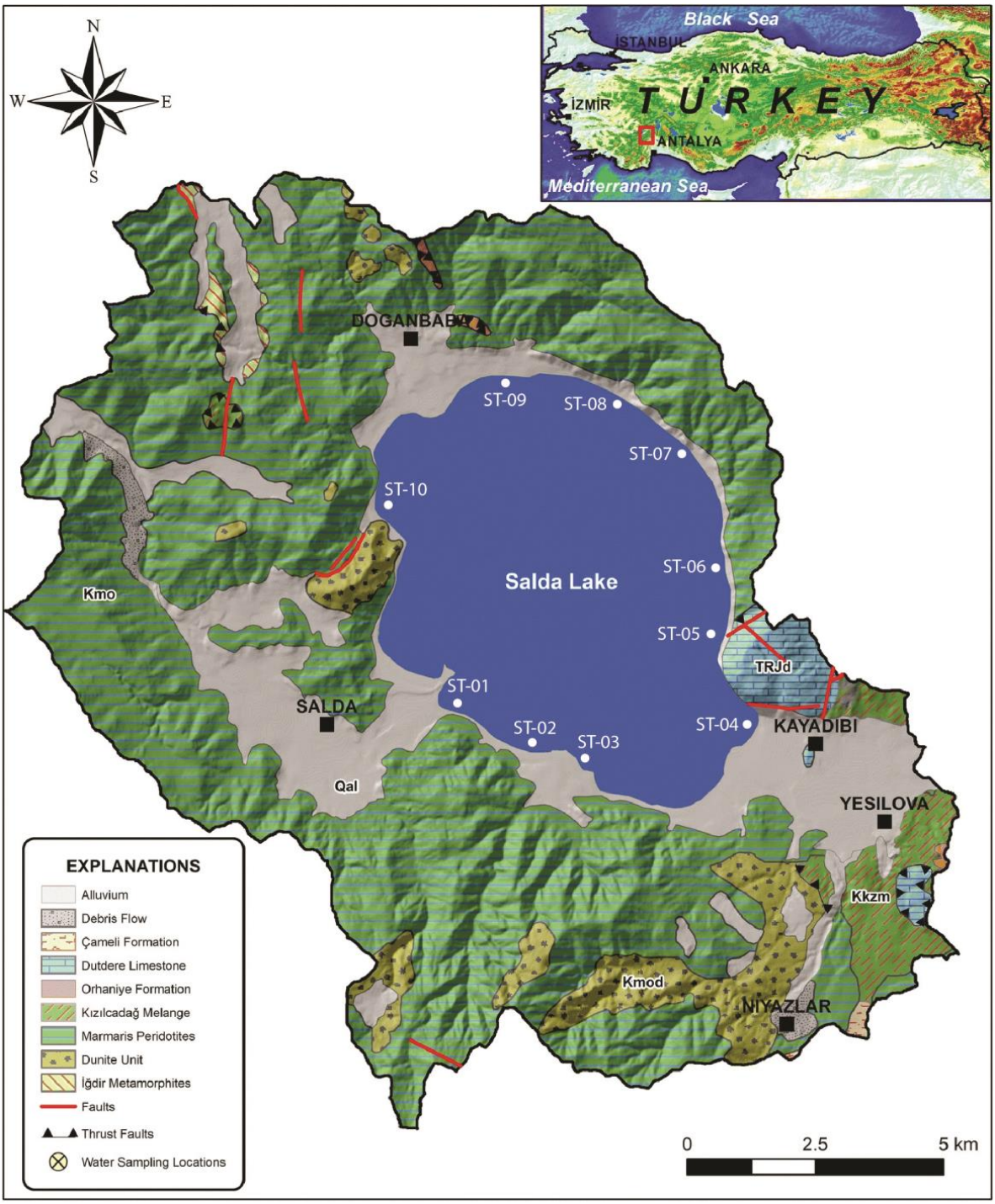

Figure 1. The geological map of the Lake Salda, SW Turkey. Adapted from Davraz, et al. [51].

Figure 2. (**a**) General view from Lake Salda, (**b**,**c**) stromatolite, (**d**) fosil stromatolite, (**e**,**f**) Serpentinized ultrabasic rock near Lake Salda and hydromagnesite in its fracture.

3. Sampling and Analytical Method

Ten stromatolite samples were collected from the water on the shoreline of Lake Salda, SW Turkey (Figure 2). Major oxides, trace elements and REEs were conducted on these samples by using a Bruker S8 Tiger model wavelength dispersive X-ray fluorescence (WD-XRF) and Perkin Elmer Elan DRC-e model inductively coupled plasma-mass spectrometry (ICP-MS), respectively, in the Geochemistry Research Laboratories of Istanbul Technical University (ITU/JAL). Powdered stromatolite samples (250 mg) were digested in two steps. The first one was completed with 6 mL of 37% HCl, 2 mL of 65% HNO3 and 1 mL of 38–40% HF in a pressure and temperature-controlled Teflon beaker using a Berghof Speedwave MWS-3^{+} model microwave at 185 °C. The second step was completed with the addition of 6 mL of 5% boric acid solution. Ce, Eu, Pr and Y anomalies for each

stromatolites were normalized to PAAS [52] by using these formulas; Ce/Ce* = Cen/$\sqrt{}$[Lan *Prn], Eu/Eu* = Eun/$\sqrt{}$[Smn *Gdn], Pr/Pr* = Prn/$\sqrt{}$[Cen *Ndn], and Y/Y* = Yn/$\sqrt{}$[Dyn *Hon]. These data were calculated statistically with variance analysis (ANOVA) and SPSS 15.0 software, by using the Student Newman Keul's Procedure [53].

The mineralogical composition of the stromatolite samples was determined at ITU/JAL by Bruker D8 Advance model X-ray diffractometer (XRD). All samples were ground up in an agate mortar and dried at room temperature. Then, the samples were collected on a silicon sample holder. Measurements were done using Cu Kα radiation with a total counting time half an hour. The MDI JADE v.0.6 software was used for the matching, background subtraction and peak identification with XRD patterns of reference compounds. As XRD analyses results, the size and abundance of the peaks of these minerals can be seen in Figure.

4. Results

4.1. Salda Lake Water

The concentration of major elements, pH, Eh and electric conductivity (EC) are reported in Table 1. The lake water had pH between 9.26 and 9.52, EC between 2.12 and 2.62 mS/cm, and Eh between −152 and −183 mV. Considering the major element concentrations in Table 1, cations are listed as Mg, Na, K and Ca, and anions as HCO_3, Cl, SO_4 and NO_2, in order of abundance. These results showed that the lake water is included in a dominant water group with more Mg and HCO_3.

Table 1. Anion and cation analysis results of lake water in Salda.

	pH	EC	Eh	Al	Si	B	Br	Cl	NO_2	SO_4	HCO_3	Ca	K	Fe	Mg	Na
		mS/cm	mV	µg/L	µg/L	µg/L	µg/L	mg/L	mg/L	mg/L	mg/L	mg/L	mg/L	mg/L	mg/L	mg/L
SL-01	9.49	2.62	−166	52	400	104	929	192	2.06	15.6	685	4.34	27.8	44	281	225
SL-02	9.33	2.18	−172	39	376	88	858	196	1.88	16.8	702	4.31	27.8	56	289	225
SL-03	9.27	2.36	−158	39	366	79	820	193	2.24	16.2	694	4.22	23.5	59	285	222
SL-04	9.52	2.55	−183	49	386	85	829	194	1.96	15.4	715	4.39	24.5	64	286	225
SL-05	9.26	2.22	−174	61	543	91	844	204	1.78	14.8	712	4.08	25.6	90	284	228
SL-06	9.33	2.38	−178	41	415	74	769	178	2.08	17.3	758	4.17	22.2	70	275	197
SL-07	9.44	2.12	−161	20	510	91	887	208	2.01	15.6	766	4.14	25.1	69	281	225
SL-08	9.38	2.44	−158	36	701	66	592	139	1.92	14.6	688	4.14	17.0	71	234	150
SL-09	9.42	2.46	−152	35	359	80	785	195	1.69	15.8	723	4.19	23.7	65	283	222
SL-10	9.36	2.28	−162	42	366	83	816	202	1.94	16.1	744	4.22	24.1	68	285	223
Avrg	9.38	2.36	−166	41	442	84.1	813	190	1.96	15.8	719	4.22	24.1	66	278	214

4.2. XRD Data

The XRD analyses were carried out for the identification of various primary and secondary mineral species in the stromatolite samples. They reveal that the stromatolites consist mainly of hydromagnesite with subordinate amount of aragonite, chrysotile, and quartz (Figure 3).

4.3. Major Oxides

As given in Table 2, the stromatolites have a variable amounts of MgO ranging from 37.6 to 42.5 wt.% with a mean of 41.2%. Loss on ignition (CO_2) vary from 48.9 to 56.6 wt.% with an average of 53.9 wt.%. The other major oxides of the stromatolites have the range of 0.22–7.88 wt.% for SiO_2, 0.02–0.92 wt.% for Al_2O_3, 0.96–1.85 wt.% for CaO, 0.02–0.13 wt.% for Na_2O, 0.01–0.11 wt.% for K_2O, 0.01–0.03 wt.% for MnO, 0.01–0.07 wt.% for TiO_2, 0.01–0.03 wt.% for P_2O_5, and 0.06 to 2.10 wt.% for Fe_2O_3 (Table 2 and Figure 4). MgO/CaO ratios of stromatolites vary from 22 to 42 with an average of 33.4. Bivariate plots for n = 10 stromatolite samples, of MgO versus CO_2, Al_2O_3 versus SiO_2, Al_2O_3 versus Na_2O, Al_2O_3 versus K_2O, Al_2O_3 versus MnO, Fe_2O_3 versus K_2O, TiO_2 versus K_2O, SiO_2 versus Fe_2O_3 and SiO_2 versus TiO_2 show high positive values (Figure 5) whereas MgO versus K_2O, Fe_2O_3, TiO_2, SiO_2, MnO, V, Cr, Cu, and Y indicate strong negative correlations (Figure 6).

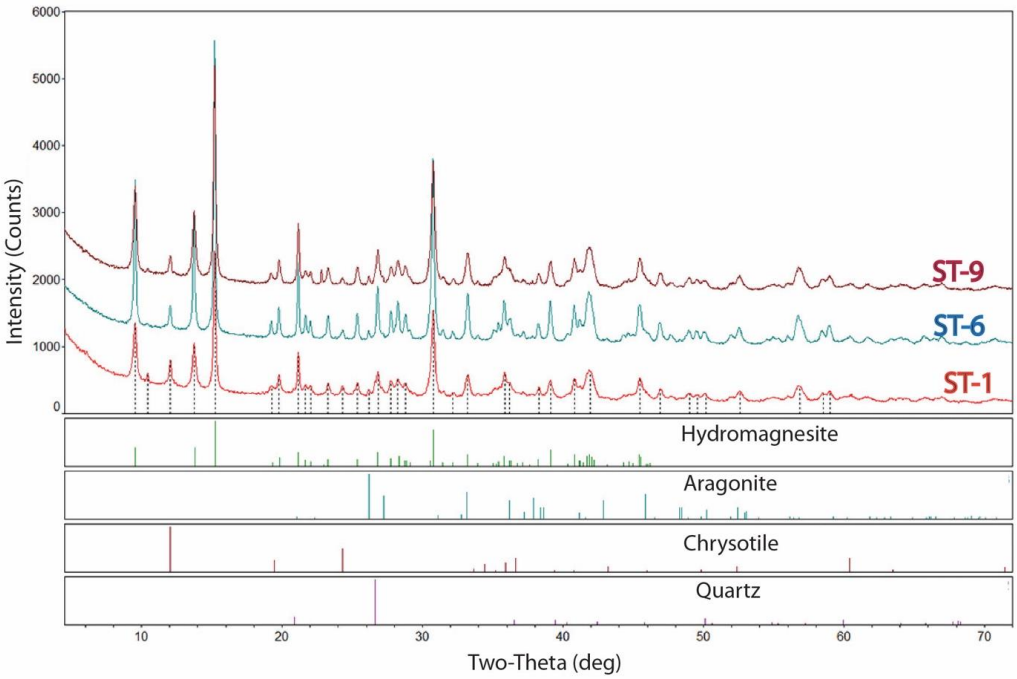

Figure 3. Representative X-ray diffraction pattern of the stromatolite samples in Lake Salda for ST-1, ST-6 and ST-9 samples.

Table 2. Major oxide contents of the stromatolites from Lake Salda, in weight percent (wt.%).

Sample No	ST 1	ST 2	ST 3	ST 4	ST 5	ST 6	ST 7	ST 8	ST 9	ST 10	Average
SiO_2	7.88	1.29	4.10	0.52	0.22	1.92	0.93	2.45	2.41	1.81	2.35
Al_2O_3	0.92	0.13	0.46	0.05	0.02	0.12	0.04	0.16	0.20	0.10	0.22
MgO	37.60	40.90	40.10	41.10	41.60	42.50	41.80	42.20	42.30	42.30	41.24
CaO	1.44	1.19	0.96	1.85	1.08	1.21	0.99	1.50	1.28	1.30	1.28
Na_2O	0.13	0.02	0.13	0.03	0.08	0.06	0.04	0.12	0.02	0.03	0.07
K_2O	0.11	0.01	0.05	0.01	0.01	0.02	0.01	0.03	0.03	0.01	0.03
MnO	0.03	0.01	0.02	0.01	0.02	0.01	0.02	0.01	0.02	0.01	0.02
Fe_2O_3	2.10	0.25	0.96	0.06	0.26	0.53	0.17	0.69	0.71	0.27	0.60
TiO_2	0.07	0.01	0.04	0.01	0.01	0.01	0.01	0.02	0.02	0.01	0.02
P_2O_5	0.01	0.01	0.01	0.01	0.01	0.01	0.01	0.02	0.01	0.03	0.01
SO_3	0.32	0.13	0.25	0.03	0.02	0.06	0.15	0.15	0.14	0.05	0.13
Cl	0.09	0.02	0.09	0.03	0.02	0.05	0.03	0.10	0.05	0.01	0.05
LOI	48.9	55.9	52.7	56.4	56.6	53.5	55.9	52.4	52.7	54.1	53.9
Total	99.6	100.0	99.9	100.0	99.9	100.0	100.0	99.9	99.9	100.0	99.9
MgO/CaO	26.11	34.37	41.77	22.22	38.52	35.12	42.22	28.13	33.05	32.54	33.41

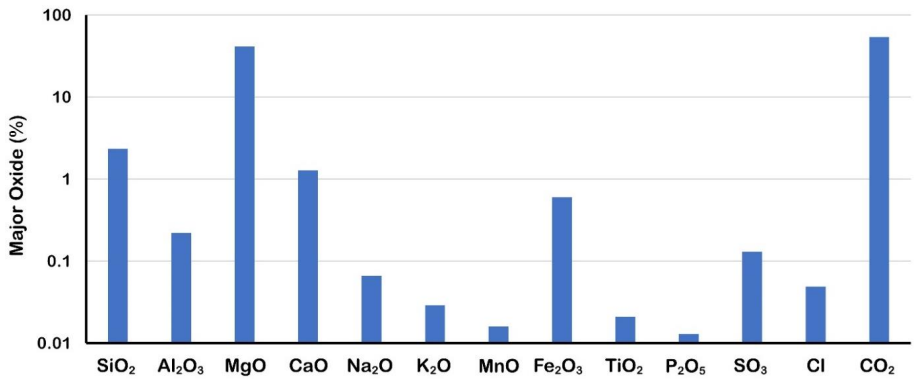

Figure 4. Major oxide contents (%) of the stromatolite samples from Lake Salda.

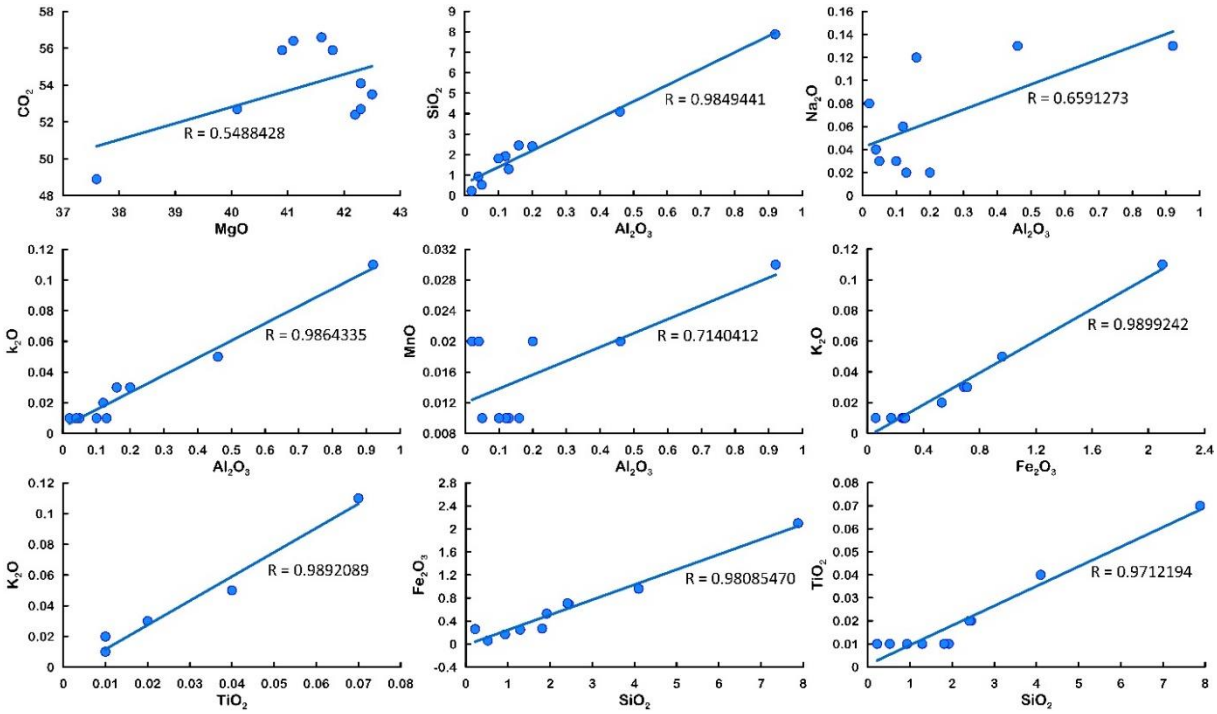

Figure 5. Positive correlation between some selected major oxides of stromatolites.

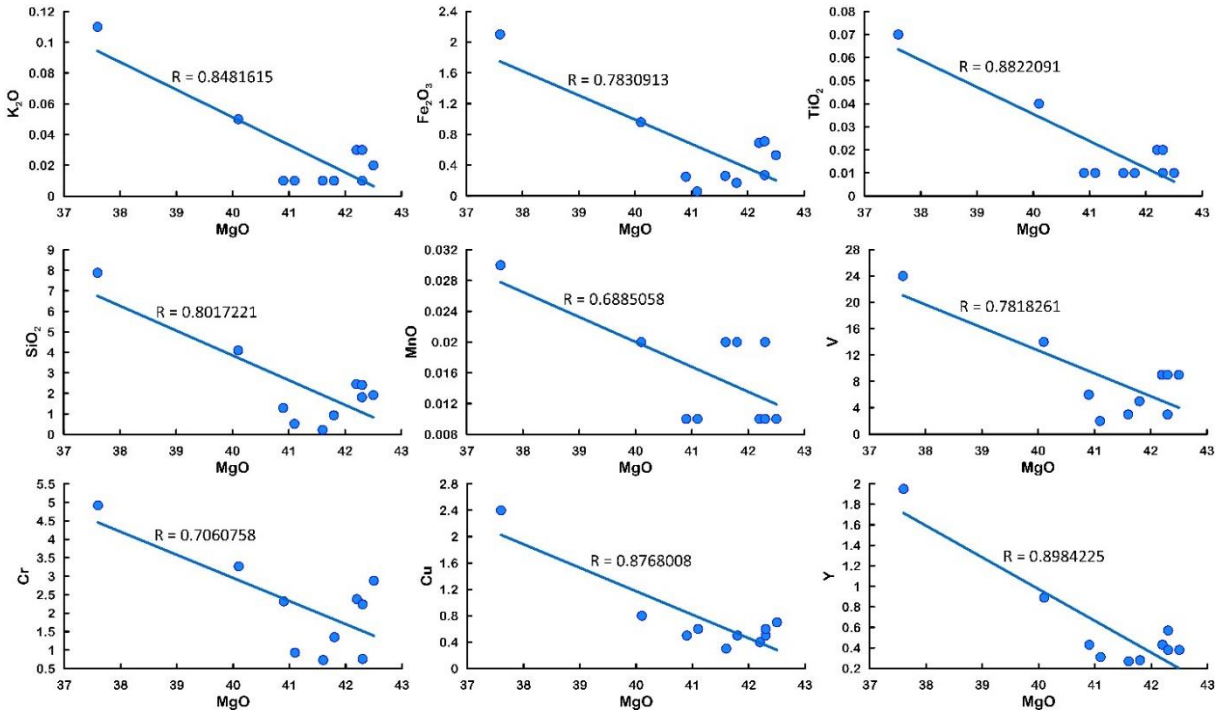

Figure 6. Negative correlations between MgO and some selected major oxides and trace elements of stromatolites.

4.4. Trace Elements

The trace element concentrations of ten stromatolites are shown in Table 3. The total trace element (∑TE) contents of the stromatolites range from 81 to 320 ppm with a mean of 208 ppm. Mean levels for the trace elements as ppm are Cr (2.18), V (8.4), Co (3.5), Ni (95.6), Cu (0.73), Rb (1.55), Sr (37.6), Y (0.59), Zr, (17.7), Nb (3.6), Ba (21), Hf (0.05), As (3.5), Cd (0.02), U (0.04), Th (0.07), Pb (2.85) and Zn (6.6). In compared to PAAS (Figure 7), the

stromatolite samples have more As and Ni, and lower V, Co, Cr, Rb, Cu, Y, Sr, Nb, Ba, Zr, Cd, Hf, Th, U, Zn and Pb concentrations [52]. The average Zr/Hf, V/Cr, Ni/Co, U/Th, and V/V+Ni ratios in the stromatolites are 340, 3.86, 5.28, 0.59, and 0.09, respectively (Table 3). Strong linear correlations among the trace elements in the studied samples were detected in Ni-V, Ni-Cr, Ni-Co, Ni-Cu, Ni-Rb, Ni-Y, Y-V, Co-Rb, Hf-Th, As-Pb, Zn-Rb, Zn-Y, Zn-Zr, Hf-V and Y-Th (Table 4).

Table 3. Trace element contents of the stromatolites from Lake Salda, in parts per million (ppm; μg g^{-1}).

Sample No	ST 1	ST 2	ST 3	ST 4	ST 5	ST 6	ST 7	ST 8	ST 9	ST 10	Average
V	24.00	6.00	14.00	2.00	3.00	9.00	5.00	9.00	9.00	3.00	8.40
Cr	4.92	2.32	3.27	0.93	0.73	2.88	1.35	2.38	2.24	0.76	2.18
Co	23.00	10.00	24.00	7.00	4.00	19.00	13.00	25.00	22.00	14.00	16.10
Ni	140.00	47.00	165.00	24.00	9.00	111.00	35.00	137.00	138.00	65.00	87.10
Cu	2.40	0.50	0.80	0.60	0.30	0.70	0.50	0.40	0.50	0.60	0.73
Rb	5.99	0.62	2.35	0.58	0.39	1.25	0.70	1.06	1.58	1.00	1.55
Sr	40.00	37.00	26.00	42.00	29.00	33.00	36.00	50.00	48.00	35.00	37.60
Zr	26.00	15.00	19.00	14.00	14.00	16.00	24.00	18.00	16.00	15.00	17.70
Nb	3.00	2.00	3.00	2.00	2.00	2.00	13.00	3.00	4.00	2.00	3.60
Ba	30.00	18.00	36.00	20.00	15.00	16.00	18.00	22.00	20.00	15.00	21.00
Hf	0.26	0.03	0.02	0.04	0.01	0.03	0.04	0.04	0.03	0.02	0.05
As	3.00	1.00	1.00	16.00	1.00	3.00	2.00	3.00	3.00	2.00	3.50
Cd	0.01	0.04	0.01	0.01	0.01	0.04	0.01	0.01	0.01	0.01	0.02
U	0.10	0.04	0.04	0.03	0.02	0.04	0.05	0.03	0.04	0.03	0.04
Th	0.12	0.07	0.06	0.04	0.05	0.07	0.08	0.06	0.07	0.05	0.07
Pb	0.60	0.80	0.40	21.00	1.20	0.80	1.60	0.90	0.40	0.80	2.85
Zn	19.0	3.0	9.0	1.0	2.0	6.0	5.0	8.0	9.0	4.0	6.6
Zr/Hf	100	500	950	350	1400	533	600	450	533	750	617
V/Cr	4.88	2.59	4.28	2.15	4.11	3.13	3.70	3.78	4.02	3.95	3.66
Ni/Co	6.09	4.70	5.89	3.43	2.25	5.84	2.69	5.48	6.27	4.64	4.73
U/Th	0.83	0.57	0.67	0.75	0.40	0.29	0.50	0.50	0.86	0.60	0.60
V/V+Ni	0.15	0.11	0.08	0.08	0.25	0.08	0.13	0.06	0.06	0.04	0.10
∑TE	324.4	143.9	304.8	151.5	82.0	221.2	155.6	280.3	274.4	158.7	209.7

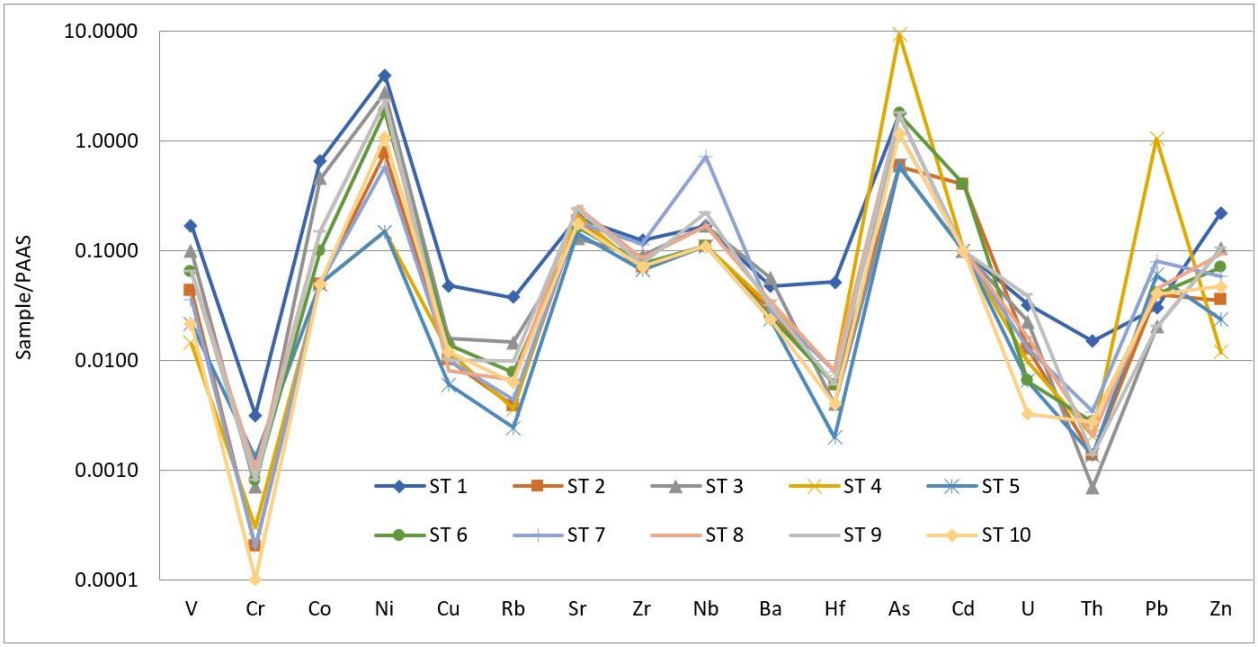

Figure 7. PAAS-normalized [52] trace element distribution of Lake Salda stromatolites.

Table 4. Correlation coefficients (R) between trace elements from the stromatolites from the Lake Salda.

	V	Cr	Co	Ni	Cu	Rb	Sr	Y	Zr	Nb	Ba	Hf	As	Cd	U	Th	Pb	Zn
V	1																	
Cr	0.96	1																
Co	0.72	0.73	1															
Ni	0.75	0.77	0.97	1														
Cu	0.87	0.79	0.40	0.42	1													
Rb	0.95	0.86	0.57	0.60	0.97	1												
Sr	0.05	0.06	0.31	0.21	0.02	0.05	1											
Y	0.95	0.86	0.53	0.57	0.96	0.99	0.03	1										
Zr	0.72	0.63	0.48	0.37	0.70	0.71	0.04	0.69	1									
Nb	−0.07	−0.12	0.01	−0.17	−0.09	−0.09	0.03	−0.12	0.60	1								
Ba	0.76	0.72	0.62	0.70	0.56	0.68	−0.12	0.71	0.53	−0.05	1							
Hf	0.82	0.74	0.35	0.33	0.96	0.92	0.20	0.92	0.73	−0.01	0.45	1						
As	−0.26	−0.26	−0.30	−0.29	−0.01	−0.13	0.33	−0.13	−0.25	−0.15	−0.06	0.03	1					
Cd	−0.07	0.17	−0.11	−0.07	−0.11	−0.20	−0.18	−0.19	−0.28	−0.25	−0.31	−0.16	−0.18	1				
U	0.86	0.80	0.43	0.40	0.94	0.91	0.10	0.90	0.84	0.19	0.51	0.94	−0.11	−0.05	1			
Th	0.83	0.80	0.47	0.42	0.82	0.83	0.12	0.81	0.84	0.28	0.39	0.85	−0.34	0.07	0.95	1		
Pb	−0.37	−0.36	−0.45	−0.43	−0.09	−0.23	0.19	−0.22	−0.30	−0.13	−0.08	−0.07	0.98	−0.17	−0.20	−0.43	1	
Zn	0.96	0.89	0.76	0.76	0.86	0.95	0.21	0.92	0.75	0.02	0.67	0.84	−0.27	−0.21	0.86	0.85	−0.40	1

4.5. Rare Earth Elements

The ∑REE contents of the stromatolite samples are between 0.95 and 5.50 ppm (an average of 1.90 ppm). The stromatolites that have higher Si and Al contents have a higher amount of ∑REE (Table 5). The PAAS [52]-normalized REE patterns of the stromatolites have a nearly horizontal trend with slight enrichment of the HREEs and depletion of the LREEs through the medium REEs (MREEs) (Figure 8). Moreover, the LaN/YbN ratios vary from 0.10 to 0.79 (mean: 0.21) indicating the HREEs enrichment and it is used to show the fractionation of the light and heavy REEs. The Er/Nd ratios vary from 0.10 to 2.50 with a mean of 0.44. The stromatolite samples have a strong negative Ce anomaly ($Ce/Ce^* = Cen/\sqrt{[Lan * Prn]}$) ranging from 0.37 to 0.64 with an average of 0.48 that shows that rock-forming minerals were primarily biogenic and marine chemical sediments. The Positive Eu anomaly ($Eu/Eu^* = Eu_n/\sqrt{[Sm_n * Gd_n]}$) varies from 1.08 to 2.64 (mean: 1.83) indicating the existence of Eu^{2+} during precipitation of the stromatolites. On the other hand, the negative Y anomaly ($Y/Y^* = Y_n/\sqrt{(Dy_n * Ho_n)}$) ranges from 0.02 to 0.06 (mean: 0.04) and negative Pr anomaly ($Pr/Pr^* = Pr_n/\sqrt{(Ce_n * Nd_n)}$) has the average of 0.86 (Table 5). The $(Y/Ho)_N$ values are between 0.50 and 2.0 with an average of 1.03 (Table 5).

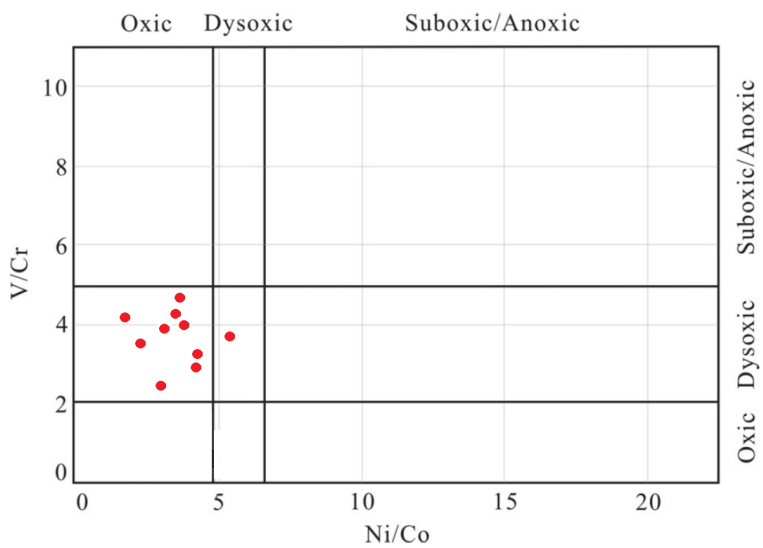

Figure 8. V/Cr vs. Ni/Co trace element ratios of stromatolites to find the redox conditions [54].

Table 5. Rare earth element (REE) contents of the stromatolites from Lake Salda, in parts per million (ppm; μg g^{-1}).

	ST 1	ST 2	ST 3	ST 4	ST 5	ST 6	ST 7	ST 8	ST 9	ST 10	Average
La	1.38	0.88	0.62	0.36	0.32	0.64	0.56	0.42	0.78	0.75	0.67
Ce	1.45	0.37	0.56	0.26	0.28	0.42	0.28	0.35	0.75	0.38	0.51
Pr	0.26	0.03	0.09	0.04	0.04	0.05	0.04	0.06	0.08	0.03	0.07
Nd	0.92	0.02	0.28	0.06	0.04	0.16	0.08	0.19	0.21	0.12	0.21
Sm	0.37	0.05	0.07	0.06	0.02	0.06	0.05	0.05	0.08	0.07	0.09
Eu	0.08	0.03	0.02	0.02	0.01	0.02	0.02	0.01	0.03	0.02	0.03
Gd	0.22	0.05	0.08	0.04	0.02	0.05	0.02	0.01	0.06	0.03	0.06
Tb	0.05	0.03	0.02	0.03	0.02	0.01	0.01	0.02	0.03	0.02	0.02
Dy	0.33	0.04	0.06	0.03	0.05	0.01	0.01	0.07	0.08	0.02	0.07
Y	0.07	0.02	0.03	0.02	0.02	0.01	0.01	0.02	0.02	0.01	0.02
Ho	0.06	0.02	0.03	0.02	0.03	0.01	0.02	0.01	0.02	0.01	0.02
Er	0.09	0.05	0.06	0.02	0.02	0.02	0.01	0.02	0.05	0.02	0.04
Tm	0.03	0.02	0.02	0.02	0.03	0.01	0.02	0.02	0.03	0.02	0.02
Yb	0.16	0.04	0.09	0.03	0.05	0.03	0.05	0.04	0.04	0.06	0.06
Lu	0.03	0.02	0.01	0.02	0.01	0.01	0.01	0.02	0.02	0.01	0.02
∑REE	5.5	1.67	2.04	1.03	0.96	1.51	1.19	1.31	2.28	1.57	1.9
$(Dy/Sm)_N$	0.79	0.02	0.28	0.12	0.12	0.16	0.16	0.1	0.21	0.12	0.21
Ce/Ce*	0.56	0.35	0.53	0.47	0.55	0.47	0.37	0.49	0.64	0.41	0.48
Eu/Eu*	1.08	2.07	1.22	1.89	2.09	1.74	2.64	1.55	2.02	1.95	1.83
Y/Y*	0.04	0.05	0.05	0.03	0.02	0.02	0.04	0.06	0.04	0.06	0.04
Pr/Pr*	0.93	0.69	0.91	1.09	1.1	0.74	0.96	0.94	0.72	0.52	0.86
Y/Ho	1.17	1	1	1	0.67	1	0.5	2	1	1	1.03
$(Yb/Gd)_N$	16.67	50	33.33	50	33.33	100	50	100	50	100	58.33
$(La/Gd)_N$	13.14	1	9.33	6	4	16	8	9.5	10.5	12	8.95
$(La/Sm)_N$	18.4	0.67	14	2	2	16	8	9.5	7	6	8.36
$(Dy/Sm)_N$	1.8	1.67	3	0.67	1	2	1	1	1.67	1	1.48

5. Discussion

Salda Lake which is located in Yesilova District (Burdur) in the southwestern Turkey is characterized by high alkaline (pH ~ 9) freshwater lake formed due to the geodynamic processes (Figure 1). The lake water is composed mainly of magnesium and carbonate that dissolved from the surrounded serpentinite harzburgite of the Upper Cretaceous Yesilova ophiolites when the passage of meteoric waters through them with the dunite outcrops and ambient sediments [13,21,22,48–50]. In addition to the ophiolites, the Upper Cretaceous carbonates that occurred on the eastern shores of the lake have also affected the alkalinity of the lake water [21,48,55]. On another hand, the proliferation of phytoplankton (diatom, blue—green algae) life, which is the most basic link of the food chain in the lake environment, causes the biological reactions positively leading to Mg-calcite precipitation [21]. The Mg elements were dissolved from the surrounding rock units transported to the Salda Lake by the meteoric water as well as by cyanobacteria and diatoms (e.g., blue-green algae) causing hydromagnesite precipitations. Balci, et al. [21] developed geomicrobiological model for Salda Lake and stated that the hydromagnesite precipitation is controlled by cyanobacteria that consumed the CO_2 and bonded the Mg+2 ions in the water to the cell membrane by the biological activities. Based to the remote sensing studies of Garczynski, et al. [3], the Jezero Crater (located in Mars) resembles Salda Lake in the geological features e.g., lithological units around the crater, hydrated Mg carbonate deposits within the crater, and fluvial channels feeding the crater.

5.1. Major Oxides

Stromatolites are biogenic rocks containing abundant CO_3^{2-} ions in water formed by bacterial activity and represent one of the oldest fossil forms of primitive life forms forming in different environments [11,33,56,57]. The geochemistry of carbonates has been often used as a proxy for the examination of geochemical marks of early or first life in the

Paleoproterozoic oceans. New analytical approaches on carbonates performed in the last years have facilitated the understanding of the interaction between carbonate precipitation and biological activity [24,37,58–65]. Although the stromatolites have different chemical compositions [13,15–19,66–71], the stromatolites in Salda Lake have higher MgO and CO_2 (CO_2+OH), and low SiO_2, CaO, Fe_2O_3, Al_2O_3 and Na_2O contents. In compared to other stromatolites of Zhao, et al. [72], Zhao, et al. [73] and Feng, et al. [74], the studied stromatolites have hydromagnesite composition [$Mg_5(CO_3)_4(OH^-)_2.4H_2O$] with an average 95.1 wt% that like the chemical composition of Dujiali Lake stromatolites, Central Qinghai-Tibetan Plateau [18,35].

5.2. Trace Elements

The average total trace element contents of the stromatolites are 209.7 ppm which are lower than those of the marine sediments (760 ppm) [75]. The Salda Lake Water is generally fed from small streams and rivers in the area where serpentinized basic/ultrabasic rocks outcropping around the lake. Therefore, both lake waters and stromatolites are enriched by the trace elements e.g., Ni, Co, Zn dissolved from the serpentinized rocks [21]. Boveiri Monji, et al. [76] concluded that Zr and Hf have great affinity for organic surfaces such stromatolite or microbial mats. The Zr/Hf values of the studied stromatolites are higher amount ranging from 100 to 1400 with a mean of 616.6 referring to favorable removal of Zr with respect to Hf. That refers also to Zr/Hf fractionations which are affected by the microbial activity in the stromatolites [77]. In compared to PAAS [52], the stromatolite samples have more As and Ni, and lower V, Co, Cr, Rb, Cu, Y, Sr, Zr, Nb, Hf, Ba, U, Cd, Zn, Th, and Pb concentrations (Figure 7). The low Ni/Co versus V/(V+Ni) [78] and Ni/Co versus V/Cr ratios [54] of the studied stromatolites indicate that they were deposited in the oxic-dysoxic zone of the lake (Figures 8 and 9). Trace element concentrations of carbonate deposits are used frequently to investigate the redox conditions [79,80]. U/Th ratio is lower than 1.25, it explains the oxic depositional environment [81]. In this context, the U/Th ratios of Salda stromatolites are between 0.29 and 0.86 (Table 3) also showing the precipitation occurred in oxic environment. The V/(V+Ni) ratio has been studied often to investigate the paleoredox conditions of carbonate minerals [82]. The average V/(V+Ni) ratio of the stromatolite samples range from 0.09 to 0.5 indicating that the stromatolite precipitation performed in oxic conditions (Figure 9).

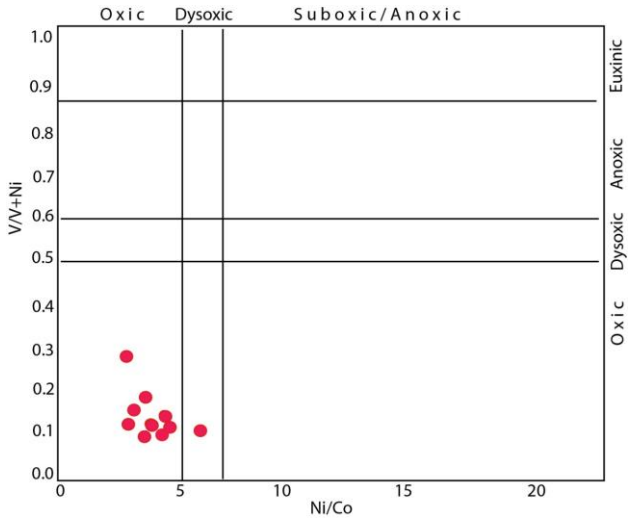

Figure 9. The V/(V+Ni) vs. Ni/Co trace element ratios of stromatolites to find the redox conditions [78].

5.3. Rare Earth Elements

The REE contents are used commonly to investigate the physicochemical conditions of precipitation environment [80,83]. PAAS normalized REE patterns of the studied stro-

matolites are mostly depleted showing that they are dissolved from the country basic and ultrabasic rocks [80,84,85]. In addition, the Er/Nd ratios higher than 0.1 show that no additional clastic material is introduced during the diagenetic process [86]. The (La/Yb)n values are similar to the terrigenous material values of Sholkovitz (1990) indicating that the LREEs are depleted by the carbonate minerals or stromatolites [87].

The ∑REE contents (mean: 1.90 ppm) of the stromatolite samples are very low because of lower REE contents of Salda Lake. The highest total REE contents in the stromatolites are observed in samples with high Al and Si. Although the Salda lake stromatolites have lower REE concentrations compared to other modern lake stromatolites [27,88], the REE trend indicates a slight horizontal with slightly increase of medium and heavy REEs (Figure 10) when normalized to PAAS referring to the studied stromatolites deposited in a confined basin where water chemistry was strongly affected by local serpantinized ultrabasic rocks.

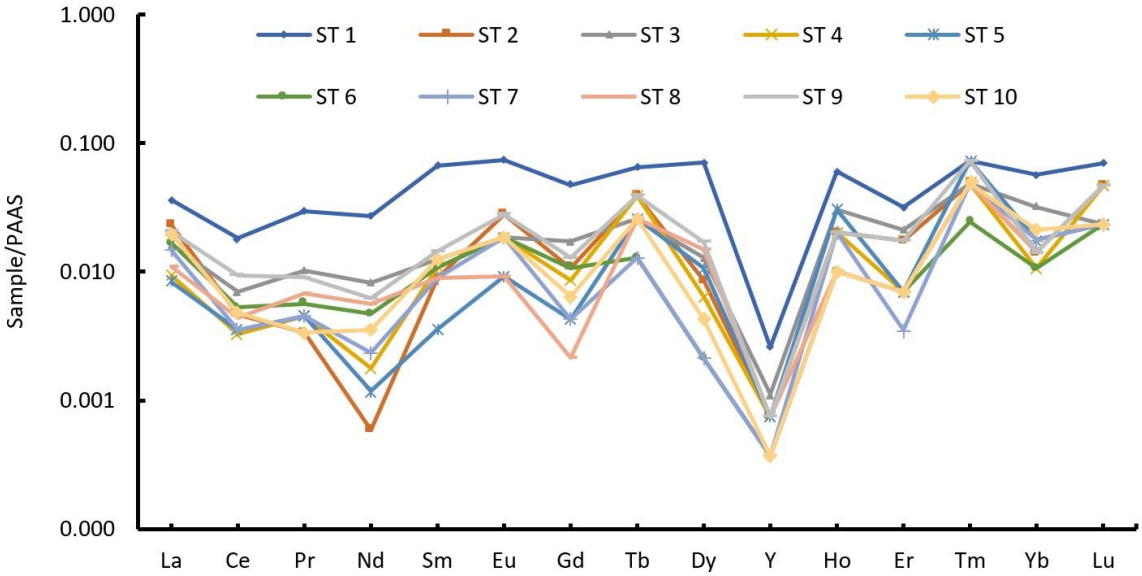

Figure 10. PAAS-normalized [52] REE + Y patterns of the Lake Salda stromatolites.

The Eu/Eu* and Ce/Ce* ratios can be used to investigate the oxygen fugacity, pH, temperature, and redox conditions of the precipitation environment [89,90]. The stromatolite samples have strong negative Ce anomalies having affinities of biogenic or marine chemical rocks. Mao, et al. [91] stated that the Ce anomaly >1 indicates an anoxic condition while <1 indicates an oxic environment depending on the oxidizing conditions. Under oxidizing conditions, Ce oxidized to Ce+4 from Ce+3 and then adsorbed by carbonates or oxides [92]. To understand the precipitation redox situation, Ce anomalies are frequently applied because Ce solubility and valences change according to redox condition. Also, when Ce is oxidized under oxidation conditions, it has negative anomalies by separating from other REEs [93]. The high negative Ce anomalies can be associated with high positive La anomalies in marine sediments. For this reason, most of the studied stromatolites can slightly show positive La anomaly [93,94]. In a Ce/Ce* vs. Pr/Pr* plot, Bau and Dulski [93] indicate that some combination of Ce and Pr anomalies actually represent positive La anomalies rather than negative Ce anomalies. All the studied stromatolites have strong negative Ce anomalies which vary from 0.35 to 0.64 with mean of 0.48, point out rapid precipitation [95,96]. Ce is removed from aqueous phase under oxidising conditions but the process is not irreversible since it depends from the aqueous REE speciation, as previously mentioned, therefore, it is considered the most important element to better understand the redox conditions during the precipitation [97]. Carbonates have typically negative Ce anomaly and low REE contents identical to seawater [98]. Positive Eu anomaly may cause by both hydrothermal solution originating in a deep-sea environment and diagenetic changes [99,100]. The studied stromatolites have Y/Ho ratios varying from 0.50 to 2.0

which are lower than those of in the marine carbonates (23–57) of [97]. The REE+Y pattern of the Lake Dujiali hydromagnesite deposits (central Qinghai-Tibetan Plateau) is similar of those of Lake Salda showing strong negative Ce and positive Eu anomalies and MREE and HREE enrichements [18,35]. Moreover, it has also been argued that the positive Eu anomaly observed in the studied hydromagnesite may be due to host ultramafic rocks [101] which are preferentially dissolved reflecting the variable effect of liquid-rock interaction [19]. Also, the positive Eu anomaly may be caused by hydrothermal fluids observed during the mineralization process [100]. Limestones are generally precipitated in shallow marine environments, therefore, the enrichment of local feldspar or clay minerals in diagenetic areas may cause positive Eu anomalies [80]. Schwinn and Markl [102] indicated that the Eu reduction from Eu3+ to Eu2+ occurs at high temperatures, resulting in Eu enrichment in minerals relative to liquids. Zeyen, et al. [103] studied the mineralogical composition of microbialites from ten Mexican Lakes and their major and trace element contents as well as the chemical composition of the surroundin g waters and concluded that high REE + Y contents with a flat pattern of these microbialites. In contrast, lacustrine-dominated microbialites show HREE enrichment (HREE-1.38 > MREE-0.98 > LREE-0.38) with high Y/Ho ratio, negative Ce anomaly and positive Eu anomaly. Subchondritic Y/Ho values probably result from the larger Ho affinity towards crystallising carbonates, especially aragonite, rather than Y [104,105].

6. Conclusions

The geochemical signatures of the stromatolites collected from Lake Salda provide significant information about the depositional environment of these stromatolites. The major oxide contents of stromatolite samples have MgO (37.6–42.46 wt.%) and CO_2 (48.9–56.59 wt.%) with less amount of SiO_2 (0.22–7.88 wt.%) and CaO (0.96–1.85 wt.%). The correlation between MgO and other oxides (SiO_2, Al_2O_3, K_2O, TiO_2, Fe_2O_3) has strong negative correlation (r = − 0.78–88), which clearly shows that Salda Lake fed lesser from different modes of origin and clastic input, except for serpentinite rocks. When trace element contents were examined according to PAAS, it was observed that it was enriched only in Ni, Co and As. The total REE contents vary from 5.50 ppm to 0.95 ppm (mean 1.90 ppm) and PAAS-normalized REE pattern of the stromatolites shows a horizontal trend or slight HREE enrichment. All stromatolites have negative Ce anomaly (mean 0.48), negative Y (0.04) anomaly and positive Eu anomaly (mean 1.83), which are consistent with precipitation in oxic conditions and partially warm lake waters. Also, all data show that the stromatolites in Lake Salda had hydromagnesite composition [$Mg_5(CO_3)4(\text{-}OH)_2.4H_2O$] containing high Ni, Co, As and low V, Cr, Rb, Cu, Y, Sr, Zr, Ba, Nb, Cd, Hf, Th, U, Zn and Pb. They have been affected by both Mg-rich meteoric waters fed from the surrounding serpentinite rocks as well as from the hydrothermal fluids with a similar composition with the lake water.

Author Contributions: Conceptualization and methodology, M.K. (Mustafa Kaya), B.A.Y., M.K. (Mustafa Kumral) and A.S.; experiment, M.K. (Mustafa Kaya), B.A.Y. and A.S; writing—original draft preparation, M.K. (Mustafa Kaya), B.A.Y. and A.S.; writing—review and editing, M.K. (Mustafa Kaya), B.A.Y., M.K. (Mustafa Kumral) and A.S.; project administration and funding acquisition, M.K. (Mustafa Kumral). All authors have read and agreed to the published version of the manuscript.

Funding: This study is supported by the Scientific Research Project (BAP project ID: 42928; Mustafa Kumral) by Istanbul Technical University (ITU, Turkey).

Data Availability Statement: The data presented in this study are available on request from the corresponding author.

Acknowledgments: We thank to Special Issue Editors, Marianna Cangemi, Salvatore Inguaggiato and anonymous reviewers for very helpful and constructive comments. This study is a part of Belgin Aydın Yıldırım's PhD Thesis. The authors would like to acknowledge the help of Chemist Beril Tanç Kaya who is a members of the Geochemistry Research Laboratories at Istanbul Technical University (ITU/JAL) for ICP-MS and XRF analysis. Also, great thanks go to Amr Abdelnasser (Benha University, Egypt) for critical reading and improving an earlier version of this manuscript.

Conflicts of Interest: The authors declare no conflict of interest.

References

1. Goudge, T.A.; Aureli, K.L.; Head, J.W.; Fassett, C.I.; Mustard, J.F. Classification and analysis of candidate impact crater-hosted closed-basin lakes on Mars. *Icarus* **2015**, *260*, 346–367. [CrossRef]
2. Goudge, T.A.; Mustard, J.F.; Head, J.W.; Fassett, C.I.; Wiseman, S.M. Assessing the mineralogy of the watershed and fan deposits of the Jezero crater paleolake system, Mars. *J. Geophys. Res. Planets* **2015**, *120*, 775–808. [CrossRef]
3. Garczynski, B.; Horgan, B.; Kah, L.; Balci, N.; Gunes, Y. Searching for potential biosignatures in Jezero Crater with Mars 2020—A spectral investigation of terrestrial lacustrine carbonate analogs. In Proceedings of the Ninth International Conference on Mars, Pasadena, CA, USA, 22–25 July 2019; p. 6302.
4. Horgan, B.H.; Anderson, R.B.; Dromart, G.; Amador, E.S.; Rice, M.S. The mineral diversity of Jezero crater: Evidence for possible lacustrine carbonates on Mars. *Icarus* **2020**, *339*, 113526. [CrossRef]
5. Karaman, M. Comparison of thresholding methods for shoreline extraction from Sentinel-2 and Landsat-8 imagery: Extreme Lake Salda, track of Mars on Earth. *J. Environ. Manag.* **2021**, *298*, 113481. [CrossRef]
6. Riu, L.; Carter, J.; Poulet, F. The M3 project: 3–Global abundance distribution of hydrated silicates at Mars. *Icarus* **2022**, *374*, 114809. [CrossRef]
7. Petryshyn, V.A.; Junkins, E.N.; Stamps, B.W.; Bailey, J.V.; Stevenson, B.S.; Spear, J.R.; Corsetti, F.A. Builders, tenants, and squatters: The origins of genetic material in modern stromatolites. *Geobiology* **2021**, *19*, 261–277. [CrossRef]
8. Allwood, A.C.; Walter, M.R.; Kamber, B.S.; Marshall, C.P.; Burch, I.W. Stromatolite reef from the Early Archaean era of Australia. *Nature* **2006**, *441*, 714–718. [CrossRef]
9. Grotzinger, J.P.; Knoll, A.H. Stromatolites in Precambrian carbonates: Evolutionary mileposts or environmental dipsticks? *Annu. Rev. Earth Planet. Sci.* **1999**, *27*, 313–358. [CrossRef]
10. Visscher, P.T.; Reid, R.P.; Bebout, B.M. Microscale observations of sulfate reduction: Correlation of microbial activity with lithified micritic laminae in modern marine stromatolites. *Geology* **2000**, *28*, 919–922. [CrossRef]
11. Reid, R.P.; Visscher, P.T.; Decho, A.W.; Stolz, J.F.; Bebout, B.; Dupraz, C.; Macintyre, I.; Paerl, H.; Pinckney, J.; Prufert-Bebout, L. The role of microbes in accretion, lamination and early lithification of modern marine stromatolites. *Nature* **2000**, *406*, 989–992. [CrossRef]
12. Dupraz, C.; Reid, R.P.; Braissant, O.; Decho, A.W.; Norman, R.S.; Visscher, P.T. Processes of carbonate precipitation in modern microbial mats. *Earth-Sci. Rev.* **2009**, *96*, 141–162. [CrossRef]
13. Braithwaite, C.; Zedef, V. Hydromagnesite stromatolites and sediments in an alkaline lake, Salda Golu, Turkey. *J. Sediment. Res.* **1996**, *66*, 991–1002.
14. Northup, E.; Kathleen, H.; Lavoie, D. Geomicrobiology of caves: A review. *Geomicrobiol. J.* **2001**, *18*, 199–222.
15. Erum, B.; Shahid, N.; Tabinda, A.; Khula, S. Characteristics of ultramafic rocks and associated magnesite deposits, Nal Area, Khuzdar, Balochistan, Pakistan. *J. Geol. Min. Res.* **2009**, *1*, 034–041.
16. Cangemi, M.; Censi, P.; Reimer, A.; D'Alessandro, W.; Hause-Reitner, D.; Madonia, P.; Oliveri, Y.; Pecoraino, G.; Reitner, J. Carbonate precipitation in the alkaline lake Specchio di Venere (Pantelleria Island, Italy) and the possible role of microbial mats. *Appl. Geochem.* **2016**, *67*, 168–176. [CrossRef]
17. Oskierski, H.; Dlugogorski, B.; Oliver, T.; Jacobsen, G. Chemical and isotopic signatures of waters associated with the carbonation of ultramafic mine tailings, Woodsreef Asbestos Mine, Australia. *Chem. Geol.* **2016**, *436*, 11–23. [CrossRef]
18. Lin, Y.; Zheng, M.; Ye, C. Hydromagnesite precipitation in the Alkaline Lake Dujiali, central Qinghai-Tibetan Plateau: Constraints on hydromagnesite precipitation from hydrochemistry and stable isotopes. *Appl. Geochem.* **2017**, *78*, 139–148. [CrossRef]
19. Power, I.M.; Wilson, S.A.; Harrison, A.L.; Dipple, G.M.; McCutcheon, J.; Southam, G.; Kenward, P.A. A depositional model for hydromagnesite–magnesite playas near Atlin, British Columbia, Canada. *Sedimentology* **2014**, *61*, 1701–1733. [CrossRef]
20. Riding, R.E.; Awramik, S.M. *Microbial Sediments*; Springer Science & Business Media: Berlin/Heidelberg, Germany, 2000.
21. Balci, N.; Demirel, C.; Kurt, M. Geomicrobiology of Lake Salda and microbial influences on present-day stromatolite formation. *Bull. Earth Sci. Appl. Res. Cent. Hacet. Univ.* **2018**, *39*, 19–40.
22. Kazanci, N.; Girgin, S.; Dügel, M. On the limnology of Salda Lake, a large and deep soda lake in southwestern Turkey: Future management proposals. *Aquat. Conserv. Mar. Freshw. Ecosyst.* **2004**, *14*, 151–162. [CrossRef]
23. Zeng, L.-Q.; Yi, H.-S.; Xia, G.-Q.; Simon, K.; Heim, C.; Arp, G. Palaeoenvironmental setting of lacustrine stromatolites in the Miocene Wudaoliang Group, northern Tibetan Plateau. *J. Palaeogeogr.* **2019**, *8*, 1–15. [CrossRef]
24. Franchi, F. Petrographic and geochemical characterization of the Lower Transvaal Supergroup stromatolitic dolostones (Kanye Basin, Botswana). *Precambrian Res.* **2018**, *310*, 93–113. [CrossRef]
25. Bonales, L.; Muñoz-Iglesias, V.; Santamaría-Pérez, D.; Caceres, M.; Fernandez-Remolar, D.; Prieto-Ballesteros, O. Quantitative Raman spectroscopy as a tool to study the kinetics and formation mechanism of carbonates. *Spectrochim. Acta Part A Mol. Biomol. Spectrosc.* **2013**, *116*, 26–30. [CrossRef]
26. Censi, P.; Cangemi, M.; Madonia, P.; Saiano, F.; Brusca, L.; Zuddas, P. Discrimination between effects induced by microbial activity and water-rock interactions under hydrothermal conditions according to REE behaviour. *Procedia Earth Planet. Sci.* **2013**, *7*, 123–126. [CrossRef]

27. Bolhar, R.; Van Kranendonk, M.J. A non-marine depositional setting for the northern Fortescue Group, Pilbara Craton, inferred from trace element geochemistry of stromatolitic carbonates. *Precambrian Res.* **2007**, *155*, 229–250. [CrossRef]
28. Frimmel, H.E. Trace element distribution in Neoproterozoic carbonates as palaeoenvironmental indicator. *Chem. Geol.* **2009**, *258*, 338–353. [CrossRef]
29. Zhao, Y.-Y.; Zheng, Y.-F.; Chen, F. Trace element and strontium isotope constraints on sedimentary environment of Ediacaran carbonates in southern Anhui, South China. *Chem. Geol.* **2009**, *265*, 345–362. [CrossRef]
30. Corkeron, M.; Webb, G.E.; Moulds, J.; Grey, K. Discriminating stromatolite formation modes using rare earth element geochemistry: Trapping and binding versus in situ precipitation of stromatolites from the Neoproterozoic Bitter Springs Formation, Northern Territory, Australia. *Precambrian Res.* **2012**, *212*, 194–206. [CrossRef]
31. Johannesson, K.H.; Telfeyan, K.; Chevis, D.A.; Rosenheim, B.E.; Leybourne, M.I. Rare earth elements in stromatolites—1. Evidence that modern terrestrial stromatolites fractionate rare earth elements during incorporation from ambient waters. In *Evolution of Archean Crust and Early Life*; Springer: Dordrecht, The Netherlands, 2014; pp. 385–411.
32. Kamber, B.S.; Webb, G.E.; Gallagher, M. The rare earth element signal in Archaean microbial carbonate: Information on ocean redox and biogenicity. *J. Geol. Soc.* **2014**, *171*, 745–763. [CrossRef]
33. Censi, P.; Cangemi, M.; Brusca, L.; Madonia, P.; Saiano, F.; Zuddas, P. The behavior of rare-earth elements, Zr and Hf during biologically-mediated deposition of silica-stromatolites and carbonate-rich microbial mats. *Gondwana Res.* **2015**, *27*, 209–215. [CrossRef]
34. Wang, S.; Magalhães, V.H.; Pinheiro, L.M.; Liu, J.; Yan, W. Tracing the composition, fluid source and formation conditions of the methane-derived authigenic carbonates in the Gulf of Cadiz with rare earth elements and stable isotopes. *Mar. Pet. Geol.* **2015**, *68*, 192–205. [CrossRef]
35. Lin, Y.; Zheng, M.; Ye, C.; Power, I.M. Trace and rare earth element geochemistry of Holocene hydromagnesite from Dujiali Lake, central Qinghai–Tibetan Plateau, China. *Carbonates Evaporites* **2019**, *34*, 1265–1279. [CrossRef]
36. Debruyne, D.; Hulsbosch, N.; Muchez, P. Unraveling rare earth element signatures in hydrothermal carbonate minerals using a source–sink system. *Ore Geol. Rev.* **2016**, *72*, 232–252. [CrossRef]
37. Franchi, F.; Hofmann, A.; Cavalazzi, B.; Wilson, A.; Barbieri, R. Differentiating marine vs hydrothermal processes in Devonian carbonatemounds using rare earth elements (Kess Kess mounds, Anti-Atlas, Morocco). *Chem. Geol.* **2015**, *409*, 69–86. [CrossRef]
38. Wang, S.; Yan, W.; Chen, Z.; Zhang, N.; Chen, H. Rare earth elements in cold seep carbonates from the southwestern Dongsha area, northern South China Sea. *Mar. Pet. Geol.* **2014**, *57*, 482–493. [CrossRef]
39. Li, R.; Jones, B. Evaluation of carbonate diagenesis: A comparative study of minor elements, trace elements, and rare-earth elements (REE + Y) between Pleistocene corals and matrices from Grand Cayman, British West Indies. *Sediment. Geol.* **2014**, *314*, 31–46. [CrossRef]
40. Loope, G.R.; Kump, L.R.; Arthur, M.A. Shallow water redox conditions from the Permian–Triassic boundary microbialite: The rare earth element and iodine geochemistry of carbonates from Turkey and South China. *Chem. Geol.* **2013**, *351*, 195–208. [CrossRef]
41. Himmler, T.; Bach, W.; Bohrmann, G.; Peckmann, J. Rare earth elements in authigenic methane-seep carbonates as tracers for fluid composition during early diagenesis. *Chem. Geol.* **2010**, *277*, 126–136. [CrossRef]
42. Sasmaz, A.; Sasmaz, B.; Hein, J.R. Geochemical approach to the genesis of the Oligocene-stratiform manganese-oxide deposit, Chiatura (Georgia). *Ore Geol. Rev.* **2021**, *128*, 103910. [CrossRef]
43. Jirsa, F.; Gruber, M.; Stojanovic, A.; Omondi, S.O.; Mader, D.; Körner, W.; Schagerl, M. Major and trace element geochemistry of Lake Bogoria and Lake Nakuru, Kenya, during extreme draught. *Geochemistry* **2013**, *73*, 275–282. [CrossRef]
44. Barrat, J.; Boulegue, J.; Tiercelin, J.; Lesourd, M. Strontium isotopes and rare-earth element geochemistry of hydrothermal carbonate deposits from Lake Tanganyika, East Africa. *Geochim. Cosmochim. Acta* **2000**, *64*, 287–298. [CrossRef]
45. Yi, H.; Lin, J.; Zhao, X.; Zhou, K.; Li, J.; Huang, H. Geochemistry of rare earth elements and origin of positive europium anomaly in Miocene-Oligocene lacustrine carbonates from Tuotuohe Basin of Tibetan Plateau. *Acta Sedimentol. Sin.* **2008**, *26*, 1.
46. Akkuş, A. Salda gölünün jeomorfolojisi. *İstanbul Üniversitesi Coğrafya Derg.* **1987**, *2*, 109–115.
47. Şenel, M.; Selçuk, H.; Bilgin, Z.; Şen, A.; Karaman, T.; Dinçer, M.; Durukan, E.; Arbas, A.; Örçen, S.; Bilgi, C. Çameli (Denizli)-Yeşilova (Burdur)-Elmalı (Antalya) ve kuzeyinin jeolojisi. *MTA Rap* **1989**, *9429*, 344.
48. Russell, M.J.; Ingham, J.K.; Zedef, V.; Maktav, D.; Sunar, F.; Hall, A.J.; Fallick, A.E. Search for signs of ancient life on Mars: Expectations from hydromagnesite microbialites, Salda Lake, Turkey. *J. Geol. Soc.* **1999**, *156*, 869–888. [CrossRef]
49. Doyen, A.; Comlekciler, F.; Kocak, K. Stratigraphic features of the Yesilova ophiolite, Burdur, south-western Turkey. In *STRATI 2013*; Springer: Cham, Switzerland, 2014; pp. 493–498.
50. Kirkayak, Y. *Salda Gölü Mars Gezegenini Keşfetme ve Anlama Görevinde Ilham Kaynagi Oldu*; TMMOB Jeoloji Mühendisleri Odası Yayınları: Ankara, Turkey, 2021.
51. Davraz, A.; Varol, S.; Sener, E.; Sener, S.; Aksever, F.; Kırkan, B.; Tokgözlü, A. Assessment of water quality and hydrogeochemical processes of Salda alkaline lake (Burdur, Turkey). *Environ. Monit. Assess.* **2019**, *191*, 1–18. [CrossRef] [PubMed]
52. Taylor, S.R.; McLennan, S.M. *The Continental Crust: Its Composition and Evolution*; Wiley–Blackwell: Hoboken, NJ, USA, 1985.
53. Sokal, R.R.; Rohlf, F. *Biometry: The Principles and Practice of Statistics in Biological Research*; W.H. Freeman and Co.: New York, NY, USA, 1995; p. 880.
54. Jones, B.; Manning, D.A. Comparison of geochemical indices used for the interpretation of palaeoredox conditions in ancient mudstones. *Chem. Geol.* **1994**, *111*, 111–129. [CrossRef]

55. Balci, N.; Gunes, Y.; Kaiser, J.; On, S.A.; Eris, K.; Garczynski, B.; Horgan, B.H. Biotic and abiotic imprints on Mg-rich stromatolites: Lessons from lake Salda, SW Turkey. *Geomicrobiol. J.* **2020**, *37*, 401–425. [CrossRef]
56. Olivier, N.; Boyet, M. Rare earth and trace elements of microbialites in Upper Jurassic coral-and sponge-microbialite reefs. *Chem. Geol.* **2006**, *230*, 105–123. [CrossRef]
57. Cangemi, M.; Bellanca, A.; Borin, S.; Hopkinson, L.; Mapelli, F.; Neri, R. The genesis of actively growing siliceous stromatolites: Evidence from Lake Specchio di Venere, Pantelleria Island, Italy. *Chem. Geol.* **2010**, *276*, 318–330. [CrossRef]
58. Nothdurft, L.D.; Webb, G.E.; Kamber, B.S. Rare earth element geochemistry of Late Devonian reefal carbonates, Canning Basin, Western Australia: Confirmation of a seawater REE proxy in ancient limestones. *Geochim. Cosmochim. Acta* **2004**, *68*, 263–283. [CrossRef]
59. Bau, M.; Alexander, B. Preservation of primary REE patterns without Ce anomaly during dolomitization of Mid-Paleoproterozoic limestone and the potential re-establishment of marine anoxia immediately after the "Great Oxidation Event". *South Afr. J. Geol.* **2006**, *109*, 81–86. [CrossRef]
60. Kamber, B.S.; Bolhar, R.; Webb, G.E. Geochemistry of late Archaean stromatolites from Zimbabwe: Evidence for microbial life in restricted epicontinental seas. *Precambrian Res.* **2004**, *132*, 379–399. [CrossRef]
61. Shields, G.A. The marine carbonate and chert isotope records and their implications for tectonics, life and climate on the early earth. *Dev. Precambrian Geol.* **2007**, *15*, 971–983.
62. Riding, R.; Fralick, P.; Liang, L. Identification of an Archean marine oxygen oasis. *Precambrian Res.* **2014**, *251*, 232–237. [CrossRef]
63. Allwood, A.C.; Kamber, B.S.; Walter, M.R.; Burch, I.W.; Kanik, I. Trace elements record depositional history of an Early Archean stromatolitic carbonate platform. *Chem. Geol.* **2010**, *270*, 148–163. [CrossRef]
64. Petrash, D.; Robbins, L.; Shapiro, R.; Mojzsis, S.; Konhauser, K. Chemical and textural overprinting of ancient stromatolites: Timing, processes, and implications for their use as paleoenvironmental proxies. *Precambrian Res.* **2016**, *278*, 145–160. [CrossRef]
65. Franchi, F.; Turetta, C.; Cavalazzi, B.; Corami, F.; Barbieri, R. Trace elements and REE geochemistry of Middle Devonian carbonate mounds (Maïder Basin, Eastern Anti-Atlas, Morocco): Implications for early diagenetic processes. *Sediment. Geol.* **2016**, *343*, 56–71. [CrossRef]
66. Zheng, M. *An Introduction to Saline Lakes on the Qinghai—Tibet Plateau*; Springer Science & Business Media: Berlin/Heidelberg, Germany, 1997; Volume 76.
67. Braithwaite, C.; Zedef, V. Living hydromagnesite stromatolites from Turkey. *Sediment. Geol.* **1994**, *92*, 1–5. [CrossRef]
68. Kazmierczak, J.; Altermann, W.; Kremer, B.; Kempe, S.; Eriksson, P.G. Mass occurrence of benthic coccoid cyanobacteria and their role in the production of Neoarchean carbonates of South Africa. *Precambrian Res.* **2009**, *173*, 79–92. [CrossRef]
69. Zedef, V.; Russell, M.J.; Fallick, A.E.; Hall, A.J. Genesis of vein stockwork and sedimentary magnesite and hydromagnesite deposits in the ultramafic terranes of southwestern Turkey: A stable isotope study. *Econ. Geol.* **2000**, *95*, 429–445. [CrossRef]
70. Power, I.M.; Wilson, S.A.; Thom, J.M.; Dipple, G.M.; Gabites, J.E.; Southam, G. The hydromagnesite playas of Atlin, British Columbia, Canada: A biogeochemical model for CO2 sequestration. *Chem. Geol.* **2009**, *260*, 286–300. [CrossRef]
71. Green, D.; Young, B. Hydromagnesite and dypingite from the Northern Pennine Orefield, northern England. *Proc. Yorks. Geol. Soc.* **2006**, *56*, 151–154. [CrossRef]
72. Zhao, Y.; Nie, F.-j.; Hou, Z.-q.; Li, Z.-q.; Zhao, X.-t.; Ma, Z.-b. Geochemistry of Targejia hot spring type cesium deposit in Tibet. *Miner. Depos. Beijing* **2007**, *26*, 163.
73. Zhao, Y.-y.; Cui, Y.-b.; Zhao, X.-t. Geological and geochemical features and significance of travertine in travertine-island from Zhabuye salt lake, Tibet, China. *Geol. Bull. China* **2010**, *29*, 124–141.
74. Feng, J.-L.; Zhao, Z.-H.; Chen, F.; Hu, H.-P. Rare earth elements in sinters from the geothermal waters (hot springs) on the Tibetan Plateau, China. *J. Volcanol. Geotherm. Res.* **2014**, *287*, 1–11. [CrossRef]
75. Turekian, K.K.; Wedepohl, K.H. Distribution of the elements in some major units of the earth's crust. *Geol. Soc. Am. Bull.* **1961**, *72*, 175–192. [CrossRef]
76. Boveiri Monji, A.; Javad Ahmadi, S.; Zolfonoun, E. Selective biosorption of zirconium and hafnium from acidic aqueous solutions by rice bran, wheat bran and platanus orientalis tree leaves. *Sep. Sci. Technol.* **2008**, *43*, 597–608. [CrossRef]
77. Censi, P.; Saiano, F.; Zuddas, P.; Nicosia, A.; Mazzola, S.; Raso, M. Authigenic phase formation and microbial activity control Zr, Hf, and rare earth element distributions in deep-sea brine sediments. *Biogeosciences* **2014**, *11*, 1125–1136. [CrossRef]
78. Hatch, J.; Leventhal, J. Relationship between inferred redox potential of the depositional environment and geochemistry of the Upper Pennsylvanian (Missourian) Stark Shale Member of the Dennis Limestone, Wabaunsee County, Kansas, USA. *Chem. Geol.* **1992**, *99*, 65–82. [CrossRef]
79. Armstrong-Altrin, J.S.; Machain-Castillo, M.L.; Rosales-Hoz, L.; Carranza-Edwards, A.; Sanchez-Cabeza, J.-A.; Ruíz-Fernández, A.C. Provenance and depositional history of continental slope sediments in the Southwestern Gulf of Mexico unraveled by geochemical analysis. *Cont. Shelf Res.* **2015**, *95*, 15–26. [CrossRef]
80. Roy, A.; Chakrabarti, G.; Shome, D. Geochemistry of the Neoproterozoic Narji limestone, Cuddapah Basin, Andhra Pradesh, India: Implication on palaeoenvironment. *Arab. J. Geosci.* **2018**, *11*, 1–13. [CrossRef]
81. Armstrong-Altrin, J.; Verma, S.P.; Madhavaraju, J.; Lee, Y.I.; Ramasamy, S. Geochemistry of upper Miocene Kudankulam limestones, southern India. *Int. Geol. Rev.* **2003**, *45*, 16–26. [CrossRef]

82. Ramos-Vázquez, M.A.; Armstrong-Altrin, J.S.; Rosales-Hoz, L.; Machain-Castillo, M.L.; Carranza-Edwards, A. Geochemistry of deep-sea sediments in two cores retrieved at the mouth of the Coatzacoalcos River delta, western Gulf of Mexico, Mexico. *Arab. J. Geosci.* **2017**, *10*, 1–19. [CrossRef]
83. Mitra, R.; Chakrabarti, G.; Shome, D. Geochemistry of the Palaeo–Mesoproterozoic Tadpatri shales, Cuddapah Basin, India: Implications on provenance, paleoweathering and paleoredox conditions. *Acta Geochim.* **2018**, *37*, 715–733. [CrossRef]
84. Sen, S.; Mishra, M. Geochemistry of Rohtas limestone from Vindhyan Supergroup, Central India: Evidences of detrital input from felsic source. *Geochem. Int.* **2015**, *53*, 1107–1122. [CrossRef]
85. Devi, K.R.; Duarah, B.P. Geochemistry of Ukhrul limestone of Assam-Arakan subduction basin, Manipur, Northeast India. *J. Geol. Soc. India* **2015**, *85*, 367–376. [CrossRef]
86. Tobia, F.H. Stable isotope and rare earth element geochemistry of the Baluti carbonates (Upper Triassic), Northern Iraq. *Geosci. J.* **2018**, *22*, 975–987. [CrossRef]
87. Nagarajan, R.; Madhavaraju, J.; Armstrong-Altrin, J.S.; Nagendra, R. Geochemistry of neoproterozoic limestones of the Shahabad formation, Bhima basin, Karnataka, southern India. *Geosci. J.* **2011**, *15*, 9–25. [CrossRef]
88. Álvaro, J.J.; Ezzouhairi, H.; Ayad, N.A.; Charif, A.; Solá, R.; Ribeiro, M.L. Alkaline lake systems with stromatolitic shorelines in the Ediacaran volcanosedimentary Ouarzazate Supergroup, Anti-Atlas, Morocco. *Precambrian Res.* **2010**, *179*, 22–36. [CrossRef]
89. Bau, M.; Moeller, P. Rare earth element fractionation in metamorphogenic hydrothermal calcite, magnesite and siderite. *Mineral. Petrol.* **1992**, *45*, 231–246. [CrossRef]
90. Bau, M. Controls on the fractionation of isovalent trace elements in magmatic and aqueous systems: Evidence from Y/Ho, Zr/Hf, and lanthanide tetrad effect. *Contrib. Mineral. Petrol.* **1996**, *123*, 323–333. [CrossRef]
91. Mao, L.; Mo, D.; Yang, J.; Guo, Y.; Lv, H. Rare earth elements geochemistry in surface floodplain sediments from the Xiangjiang River, middle reach of Changjiang River, China. *Quat. Int.* **2014**, *336*, 80–88. [CrossRef]
92. German, C.R.; Elderfield, H. Application of the Ce anomaly as a paleoredox indicator: The ground rules. *Paleoceanography* **1990**, *5*, 823–833. [CrossRef]
93. Bau, M.; Dulski, P. Distribution of yttrium and rare-earth elements in the Penge and Kuruman iron-formations, Transvaal Supergroup, South Africa. *Precambrian Res.* **1996**, *79*, 37–55. [CrossRef]
94. Xie, G.; Shen, Y.; Liu, S.; Hao, W. Trace and rare earth element (REE) characteristics of mudstones from Eocene Pinghu Formation and Oligocene Huagang Formation in Xihu Sag, East China Sea Basin: Implications for provenance, depositional conditions and paleoclimate. *Mar. Pet. Geol.* **2018**, *92*, 20–36. [CrossRef]
95. Tostevin, R.; Shields, G.A.; Tarbuck, G.M.; He, T.; Clarkson, M.O.; Wood, R.A. Effective use of cerium anomalies as a redox proxy in carbonate-dominated marine settings. *Chem. Geol.* **2016**, *438*, 146–162. [CrossRef]
96. Bau, M.; Schmidt, K.; Koschinsky, A.; Hein, J.; Kuhn, T.; Usui, A. Discriminating between different genetic types of marine ferro-manganese crusts and nodules based on rare earth elements and yttrium. *Chem. Geol.* **2014**, *381*, 1–9. [CrossRef]
97. Mazumdar, A.; Tanaka, K.; Takahashi, T.; Kawabe, I. Characteristics of rare earth element abundances in shallow marine continental platform carbonates of Late Neoproterozoic successions from India. *Geochem. J.* **2003**, *37*, 277–289. [CrossRef]
98. Polgári, M.; Hein, J.; Vigh, T.; Szabó-Drubina, M.; Fórizs, I.; Bíró, L.; Müller, A.; Tóth, A. Microbial processes and the origin of the Úrkút manganese deposit, Hungary. *Ore Geol. Rev.* **2012**, *47*, 87–109. [CrossRef]
99. Worash, G.; Valera, R. Rare earth element geochemistry of the Antalo Supersequence in the Mekele Outlier (Tigray region, northern Ethiopia). *Chem. Geol.* **2002**, *182*, 395–407. [CrossRef]
100. Abedini, A.; Calagari, A.A. Rare earth element geochemistry of the Upper Permian limestone: The Kanigorgeh mining district, NW Iran. *Turk. J. Earth Sci.* **2015**, *24*, 365–382. [CrossRef]
101. Chen, L.; Ma, T.; Du, Y.; Xiao, C. Dissolved rare earth elements of different waters in Qaidam Basin, northwestern China. *Procedia Earth Planet. Sci.* **2017**, *17*, 61–64. [CrossRef]
102. Schwinn, G.; Markl, G. REE systematics in hydrothermal fluorite. *Chem. Geol.* **2005**, *216*, 225–248. [CrossRef]
103. Zeyen, N.; Benzerara, K.; Beyssac, O.; Daval, D.; Muller, E.; Thomazo, C.; Tavera, R.; López-García, P.; Moreira, D.; Duprat, E. Integrative analysis of the mineralogical and chemical composition of modern microbialites from ten Mexican lakes: What do we learn about their formation? *Geochim. Et Cosmochim. Acta* **2021**, *305*, 148–184. [CrossRef]
104. Qu, C.; Liu, G.; Zhao, Y. Experimental study on the fractionation of yttrium from holmium during the coprecipitation with calcium carbonates in seawater solutions. *Geochem. J.* **2009**, *43*, 403–414. [CrossRef]
105. Chengli, Q.; Bo, L.; Gang, L. Enrichment of lanthanides in aragonite. *J. Rare Earths* **2009**, *27*, 1062–1065.